# Emulating multi-channel scattering based on the eigenvector continuation in the discrete basis formalism

K. Hagino, <sup>1</sup> S. Yoshida, <sup>2,3</sup> M. Kimura, <sup>3</sup> and K. Uzawa<sup>1,\*</sup>

<sup>1</sup>Department of Physics, Kyoto University, Kyoto 606-8502, Japan <sup>2</sup>School of Data Science and Management, Utsunomiya University, Mine, Utsunomiya 321-8505, Japan <sup>3</sup>RIKEN Nishina Center for Accelerator-based Science, RIKEN, Wako 351-0198, Japan

We construct an emulator for a multi-channel scattering problem based on the eigenvector continuation. To this end, we employ the Kohn variational principle formulated in the discrete basis formalism. We apply this to one-dimensional scattering problems with a Gaussian barrier. Both for a single-channel and two-channel problems, we demonstrate that the penetration probability as well as the wave functions are well reproduced by the emulator. In particular, the energy dependence of the penetrability in a wider range of energy from well below the barrier to well above the barrier is successfully reproduced.

# INTRODUCTION

An emulator provides a convenient tool to surrogate a quantum mechanical calculation. With an emulator. one can obtain an approximate solution, which however is highly accurate and quick to obtain. This significantly reduces a computational cost, providing a useful means when similar calculations have to be repeated many times. A typical application of emulators is to an uncertainty quantification [1, 2], in which one has to repeat calculations many times with different parameter sets to estimate uncertainties of a theoretical model.

The eigenvector continuation (EC) [3–5] has been a powerful tool to construct emulators. In this method, to obtain an approximate solution for a model Hamiltonian, one linearly superposes a few eigenvectors of the model Hamiltonian with several different model parameters. This method was firstly applied to bound state problems of atomic nuclei [6–15]. Recently, the eigenvector continuation has been applied also to nuclear reactions as well [16-24].

In this paper, we construct an emulator for nuclear scattering based on the eigenvector continuation together with the Kohn variational principle [25–31]. Even though the Kohn variational principle has been employed in Refs. [16, 24] to construct emulators for nuclear scattering, we reformulate it with a different formalism, that is, the discrete basis formalism [32–35]. In this formalism, a scattering problem is solved in a matrix form with a linear algebra. This has been applied to induced fission reactions [32–35] as well as to barrier penetration problems [36, 37]. An advantage of this method is that it is well compatible with many-body wave functions [38]. Recently, a new scattering theory based on the discrete basis formalism with the Kohn variational principle has been proposed in Ref. [38]. The aim of this paper is applied it to construct scattering emulators using the eigenvector continuation.

The paper is organized as follows. In Sec. II, we consider a single channel scattering with a Gaussian barrier. We first detail the discrete basis formalism for a onedimensional scattering, and then construct an emulator based on the eigenvector continuation. In Sec. III, we extend the scattering emulator to a multi-channel problem. We then summarize the paper in Sec. IV.

#### II. SINGLE-CHANNEL PROBLEM

### Discrete basis formalism

We consider a one-dimensional problem with a potential  $V(x; \boldsymbol{\theta})$ , where  $\boldsymbol{\theta}$  is a set of parameters which characterize the potential V. In this paper, we consider a Gaussian potential given by,

$$V(x; \boldsymbol{\theta}) = V_0 e^{-x^2/2s^2}, \tag{1}$$

in which the parameter set  $\theta$  consists of the height  $V_0$ and the width s of the barrier, that is,  $\theta = (V_0, s)$ . The Hamiltonian of this system is given by

$$H = -\frac{\hbar^2}{2m} \frac{d^2}{dx^2} + V(x; \boldsymbol{\theta}), \tag{2}$$

where m is the mass of a particle. We consider a situation in which the particle is incident from the left hand side of the barrier. The boundary condition then reads,

$$\phi(x) \to e^{ikx} + Re^{-ikx} \quad (x \to -\infty),$$

$$\to Te^{ikx} \quad (x \to \infty),$$
(3)

$$\rightarrow Te^{ikx} \qquad (x \rightarrow \infty), \tag{4}$$

where  $\phi(x)$  is the wave function and k is the wave number. T and R are the transmission and the reflection coefficients, respectively. The penetration probability of the barrier is given by,

$$P = |T|^2 = 1 - |R|^2, (5)$$

in which we have used the flux conservation.

Let us solve this problem with the Kohn variational principle in the discrete basis formalism [38]. For this

<sup>\*</sup> Present address: Nuclear Data Center, Japan Atomic Energy Agency, Tokai, Ibaraki 319-1195, Japan.

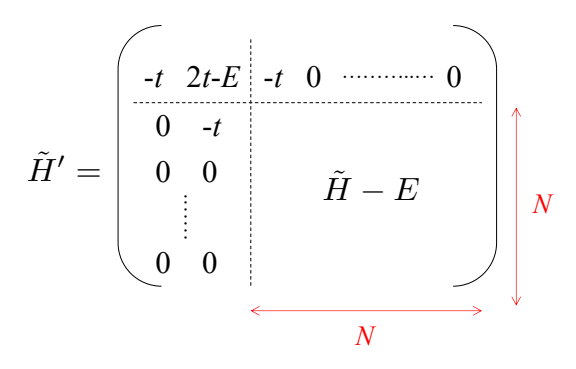


FIG. 1. A schematic illustration of the the  $(N+1) \times (N+2)$  matrix  $\tilde{H}'_{ij}$  defined by Eqs. (13)–(16).

purpose, we first discretize the coordinate x with N mesh points from  $x_{\min}$  to  $x_{\max}$ . That is, the i-th mesh point is given by  $x_i = x_{\min} + (i-1)\Delta x$  with  $i = 1, 2, \cdots, N$ , where  $\Delta x = (x_{\max} - x_{\min})/(N-1)$  is the mesh spacing. Here, the potential V is assumed to be vanishingly small at  $x_{\min}$  and  $x_{\max}$  so that the wave functions at these points satisfy the asymptotic boundary conditions, Eq. (3) and Eq. (4). Using the three-point formula for the second derivative, the Hamiltonian, Eq. (2), is represented in a matrix form as,

$$H_{ij} = -t \,\delta_{i,j+1} + (2t + V_i) \,\delta_{i,j} - t \,\delta_{i,j-1}, \qquad (6)$$

with  $i, j = 1, 2, \dots, N$ , where  $t \equiv \hbar^2/[2m(\Delta x)^2]$  and  $V_i \equiv V(x_i; \boldsymbol{\theta})$ . The wave function  $\phi_i \equiv \phi(x_i)$  then obeys the equation

$$-t\phi_0 \,\delta_{i,1} + \sum_{j=1}^{N} H_{ij}\phi_j - t\phi_{N+1}\delta_{i,N} = E\phi_i, \tag{7}$$

where E is the energy of the system. In addition, the wave function  $\phi_0$  at  $x=x_0$  satisfies the equation

$$-t\phi_{-1} + 2t\phi_0 - t\phi_1 = E\phi_0. \tag{8}$$

Notice that the wave function  $\phi_i^{(0)}$  for a free particle is given by

$$-t(\phi_{i+1}^{(0)} - 2\phi_i^{(0)} + \phi_{i-1}^{(0)}) = E\phi_i^{(0)}.$$
 (9)

Substituting  $\phi_i^{(0)} \propto e^{\pm ikx_i}$  into this equation, one obtains the dispersion relation

$$\cos(k\Delta x) = 1 - \frac{E}{2t}.\tag{10}$$

The last term on the left hand side of Eq. (7) can be handled by noticing  $\phi_{N+1} = e^{ik\Delta x} \phi_N$  (see Eq. (4)). This is equivalent to modifying Eq. (7) to,

$$-t\phi_0 \,\delta_{i,1} + \sum_{j=1}^{N} \tilde{H}_{ij}\phi_j = E\phi_i, \tag{11}$$

where  $\tilde{H}_{ij} \equiv H_{ij}$  except for  $\tilde{H}_{NN} \equiv H_{NN} - te^{ik\Delta x}$ . The N+1 equations, Eq. (8) and Eq. (11), can be combined into

$$\tilde{H}' \begin{pmatrix} \phi_{-1} \\ \phi_{0} \\ \phi_{1} \\ \vdots \\ \phi_{N} \end{pmatrix} = 0, \tag{12}$$

where the  $(N+1)\times (N+2)$  matrix  $\tilde{H}'_{ij}$  with  $i=0,1,\cdots,N$  and  $j=-1,0,1,\cdots,N$  is defined as (see Fig. 1).

$$\tilde{H}'_{ij} = \tilde{H}_{i,j} - E \, \delta_{i,j}, \quad (i, j \ge 1),$$
 (13)

$$\tilde{H}'_{0,-1} = \tilde{H}'_{01} = \tilde{H}'_{10} = -t, \tag{14}$$

$$\tilde{H}'_{00} = 2t - E, \tag{15}$$

$$\tilde{H}'_{1,-1} = 0. (16)$$

The wave function  $\phi_0$  at  $x=x_0$  in the first term on the left hand side of Eq. (11) has both the incoming and the outgoing components (see Eq. (3)). In order to take into account this term, we employ the Kohn variational principle. For that purpose, we extend the model space by adding  $x_{-1}$  and  $x_0$ , and introduce the basis functions

$$\psi_k = (e^{-ik\Delta x}, 1, 0, \cdots, 0)^T,$$
 (17)

$$\psi_{-k} = (\psi_k)^* = (e^{ik\Delta x}, 1, 0, \dots, 0)^T,$$
 (18)

$$\psi_n = (0, 0, 0, \dots, 1, 0, \dots, 0)^T,$$
 (19)

where T represents transpose. Each of these basis functions has N+2 components, for which  $\psi_n$  with  $n=1,2,\cdots,N$  has a component of  $\psi_n(i)=\delta_{i,n+2}$ . We express the total wave function as

$$\Psi = \psi_k + b_0 \psi_{-k} + \sum_{n=1}^{N} b_n \psi_n \equiv \psi_k + \sum_{n=0}^{N} b_n \psi_n, \quad (20)$$

and impose the condition  $\tilde{H}'\Psi = 0$ . Here,  $\psi_0$  is defined as  $\psi_0 \equiv \psi_{-k}$ . Defining the  $(N+2) \times (N+1)$  wave function matrix  $\varphi_{ij} \equiv \psi_j(i)$  with  $i = -1, 0, 1, \dots, N$  and  $j = 0, 1, \dots, N$ , the condition  $\tilde{H}'\Psi = 0$  reads

$$\sum_{i=-1}^{N} \sum_{j=0}^{N} \tilde{H}'_{li} \varphi_{ij} b_{j} = -\sum_{i=-1}^{N} \tilde{H}'_{li} \psi_{k}(i) \quad (l = 0, 1, \dots, N),$$
(21)

or

$$\sum_{j=0}^{N} (\tilde{H}'\varphi)_{lj}b_j = -(\tilde{H}'\psi_k)_l \equiv -\tilde{\psi}_l \quad (l=0,1,\cdots,N).$$

The amplitudes  $\{b_i\}$  can then be obtained by inverting the  $(N+1)\times (N+1)$  matrix  $(\tilde{H}'\varphi)$  as

$$b_j = -\sum_{l=0}^{N} \left[ (\tilde{H}'\varphi)^{-1} \right]_{jl} \tilde{\psi}_l. \tag{23}$$

The penetrability (5) is then computed as,

$$P = 1 - |b_0|^2 = |b_N|^2. (24)$$

# B. Eigenvector continuation

Using the solution obtained in the previous subsection, one can construct a vector  $\phi$  defined as

$$\phi = \sum_{n=1}^{N} b_n \psi_n = (0, 0, b_1, b_2, \cdots, b_N)^T.$$
 (25)

The idea of the eigenvector continuation is to linearly superpose in Eq. (20)

$$\phi_i = (0, 0, b_1^{(i)}, b_2^{(i)}, \cdots, b_N^{(i)})^T, \tag{26}$$

obtained with the parameter set  $\theta_i$  instead of  $\psi_n$  and obtain the scattering solution for the parameter set  $\theta$ . That is,

$$\Psi = \psi_k + c_0 \psi_{-k} + \sum_{i=1}^{N_{\text{EC}}} c_i \phi_i, \tag{27}$$

where  $N_{\rm EC}$  is the number of the basis states to be superposed in the eigenvector continuation and  $\{c_i\}$  are the coefficients for the superposition. From the condition of  $\tilde{H}'\Psi = 0$ , one obtains

$$\sum_{i=0}^{N_{\rm EC}} c_j \langle \phi_i' | \tilde{H}' | \phi_j \rangle = -\langle \phi_i' | \tilde{H}' | \psi_k \rangle \equiv -d_i, \qquad (28)$$

where  $\phi_0 \equiv \psi_{-k}$  as in the previous subsection, and the function  $\phi_i'$  is defined as  $|\phi_i'\rangle \equiv \tilde{H}'|\phi_i\rangle^{-1}$ .  $d_i$  is defined as  $d_i \equiv \langle \phi_i'|\tilde{H}'|\psi_k\rangle$ . The matrix elements on the left hand side of Eq. (28) can be easily obtained by noticing that  $\Psi_i = \psi_k + b_0^{(i)}\psi_{-k} + \phi_i$  satisfies  $\tilde{H}_i\Psi_i = 0$ , where  $\tilde{H}_i$  is the matrix  $\tilde{H}$  constructed with the potential  $V(x;\boldsymbol{\theta}_i)$  and that  $\tilde{H}_i - \tilde{H}$  contains only the diagonal matrix  $[(V(x;\boldsymbol{\theta}_i) - V(x;\boldsymbol{\theta})] \mathbf{1}$ , where  $\mathbf{1}$  is the unit matrix. The coefficients  $c_i$  in Eq. (28) can be obtained by inverting the matrix  $A_{ij} \equiv \langle \phi_i'|\tilde{H}'|\phi_j\rangle$  as,

$$c_i = \sum_{j=0}^{N_{\text{EC}}} (A^{-1})_{ij} d_j.$$
 (29)

The penetrability is then computed as

$$P = 1 - |c_0|^2 = \left| \sum_{i=1}^{N_{\text{EC}}} c_i b_N^{(i)} \right|^2.$$
 (30)

Fig. 2(a) and 2(b) show the penetrability for the Gaussian barrier (1) as a function of E in the linear and

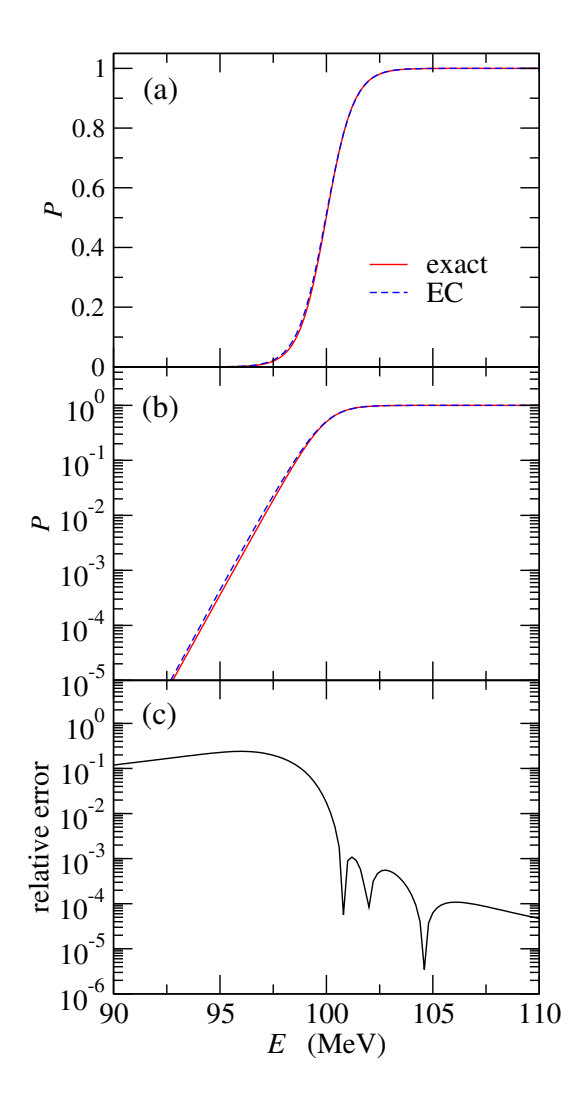


FIG. 2. (a) The penetrability of the Gaussian barrier with  $V_0=100~{\rm MeV}$  in the linear scale as a function of the energy E. The solid line shows the exact result, while the dashed line is obtained with the eigenvector continuation with  $N_{\rm EC}=4$  with  $V_0=98,~99,~101,~{\rm and}~102~{\rm MeV}.$  (b) The same as (a) but in the logarithmic scale. (c) The relative error defined by  $|P_{\rm exact}-P_{\rm EC}|/P_{\rm exact},$  where  $P_{\rm exact}$  and  $P_{\rm EC}$  are the exact penetrability and that obtained with the eigenvector continuation, respectively.

the logarithmic scales, respectively. To this end, we use  $V_0{=}100$  MeV,  $s{=}3$  fm, and  $m=29m_N,\ m_N$  being the nucleon mass, to mimic the fusion reaction of  $^{58}{\rm Ni}{+}^{58}{\rm Ni}$  [36, 39–41]. We discretize the coordinate x from  $x_{\rm min}=-20$  fm to  $x_{\rm max}{=}20$  fm with  $\Delta x=0.05$  fm. In the figure, the solid lines show the exact solution, while the dashed lines are obtained with the eigenvector continuation. For the latter, we take  $N_{\rm EC}=4$  with  $V_0=98,\ 99,\ 101,\ {\rm and}\ 102$  MeV, all with s=3 fm, and apply the eigenvector continuation at each E separately. It is remarkable that the eigenvector continuation reproduces the exact results not only around the barrier but

<sup>&</sup>lt;sup>1</sup> We have examined another choice of  $\phi'$  with  $\phi'_i = (0, b_1^{(i)}, b_2^{(i)}, \cdots, b_N^{(i)})^T$ , that is, it is the same as  $\phi_i$  but the first component is removed. We have found that this choice sometimes leads to an unstable solution, even though the flux conservation is better reproduced.

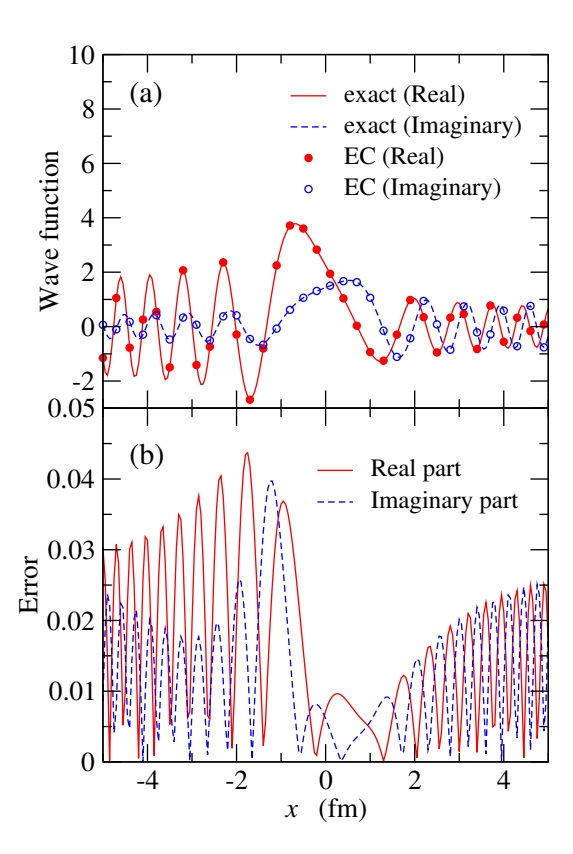


FIG. 3. (a) The wave function at the barrier top energy, E=100 MeV. The solid and the dashed lines show the real and the imaginary parts of the exact wave function,  $\Psi_{\rm exact}$ . The solid and the open circles show the real and the imaginary parts of the wave function obtained with the eigenvector continuation,  $\Psi_{\rm EC}$ . (b) The error of the wave function defined as  $|\Psi_{\rm exact} - \Psi_{\rm EC}|$ .

also well below the barrier at which the penetrability is exponentially small. Notice that the dimension of the matrix to be inverted in Eq. (23) is N+1=802, which is significantly reduced to  $N_{\rm EC}+1$ =5 in Eq. (29) in the eigenvector continuation. It is interesting to see that the exact results are yet reproduced well even with such a small number of basis. Fig. 2(c) shows the relative error  $|P_{\rm exact}-P_{\rm EC}|/P_{\rm exact}$ , where  $P_{\rm exact}$  and  $P_{\rm EC}$  are the exact penetrability and that obtained with the eigenvector continuation, respectively. One can see that the eigenvector continuation reproduces the exact result within about  $10^{-4}$  at energies above the barrier, even though the error increases to  $O(10^{-1})$  at energies below the barrier. We notice that the performance of the eigenvector continuation increases for a larger value of  $N_{\rm EC}$ .

The upper panel of Fig. 3 shows the total wave function  $\Psi$  at the barrier-top energy,  $E=V_0=100$  MeV. The solid and the dashed lines show the real and the imaginary parts of the exact wave function, and the solid and the open circles show the corresponding wave functions in the eigenvector continuation. The error of the wave functions

tion,  $|\Psi_{\rm exact} - \Psi_{\rm EC}|$ , is shown in the lower panel of Fig. 3. Here,  $\Psi_{\rm exact}$  and  $\Psi_{\rm EC}$  are the exact wave function and the wave function in the eigenvector continuation, respectively. Notice that we do not divide the error by  $\Psi_{\rm exact}$ , as it can be zero at the nordal points. One can see that the wave function is reproduced within  $O(10^{-2})$  both for the real and the imaginary parts. This accuracy is sufficient to yield the relative error of  $O(10^{-2})$  for the penetrability P, which requires only the asymptotic behaviour of the wave function.

### III. TWO-CHANNEL PROBLEM

# A. Discrete basis formalism

It is easy to extend the formalisms presented in the last section to a multi-channel problem. To demosntrate this, let us consider a two-channel problem given by,

$$\begin{split} &-\frac{\hbar^2}{2m}\,\frac{d^2}{dx^2}\begin{pmatrix}\phi_1(x)\\\phi_2(x)\end{pmatrix}\\ &+\begin{pmatrix}V(x;\pmb{\theta})&F(x;\pmb{\theta})\\F(x;\pmb{\theta})&V(x;\pmb{\theta})+\epsilon\end{pmatrix}\begin{pmatrix}\phi_1(x)\\\phi_2(x)\end{pmatrix}=E\begin{pmatrix}\phi_1(x)\\\phi_2(x)\end{pmatrix}31) \end{split}$$

where  $\phi_1(x)$  and  $\phi_2(x)$  are the scattering wave functions in the channels 1 and 2, respectively.  $F(x; \theta)$  is the coupling potential and  $\epsilon$  is the excitation energy of the channel 2. In this paper, we consider a Gaussian function for  $F(x; \theta)$ ,

$$F(x; \boldsymbol{\theta}) = F_0 e^{-x^2/2s_f^2}, \tag{32}$$

together with the Gaussian potential for V given by Eq. (1). In this case, a parameter set  $\theta$  consists of four variables,  $\theta = (V_0, s, F_0, s_f)$ . The scattering boundary conditions for the wave function  $\phi_s(x)$  (s = 1, 2) read,

$$\phi_s(x) \to e^{ik_s x} \delta_{s,1} + R_s e^{-ik_s x} \quad (x \to -\infty), \quad (33)$$
  
$$\to T_s e^{ik_s x} \quad (x \to \infty), \quad (34)$$

where  $k_s$  is the wave function for the channel s, given by  $k_1 = k$  in Eq. (10) and

$$\cos(k_2 \Delta x) = 1 - \frac{E - \epsilon}{2t}.$$
 (35)

Notice that the incident right-going wave exists at  $x = -\infty$  only for the channel 1. The penetration probability of the barrier is then given by,

$$P = |T_1|^2 + \frac{k_2}{k_1}|T_2|^2 = 1 - |R_1|^2 - \frac{k_2}{k_1}|R_2|^2.$$
 (36)

The discretized version of Eq. (31) that corresponds to Eq. (11) is given by,

$$-t\phi_{s,0}\,\delta_{i,1} + \sum_{s'=1,2} \sum_{j=1}^{N} \tilde{H}_{si,s'j}\phi_{s',j} = E\phi_{s,i}, \qquad (37)$$

where  $\phi_{s,i}$  is defined as  $\phi_s(x_i)$  and  $\tilde{H}_{si,s'i}$  is given by,

$$\tilde{H}_{si,s'j} = \left[ -t \, \delta_{i,j+1} + \left( 2t + V_i + \epsilon \, \delta_{s,2} \right) \delta_{i,j} - t \, \delta_{i,j-1} \right] \delta_{s,s'} + F_i \delta_{i,j} \delta_{s \neq s'} - t e^{ik_s \Delta x} \delta_{s,s'} \delta_{i,j} \delta_{i,N}.$$
(38)

Here  $F_i$  is defined as  $F_i \equiv F(x_i; \boldsymbol{\theta})$ , and the last term is due to the relation  $\phi_{s,N+1} = e^{ik_s\Delta x}\phi_{s,N}$  (see Eq. (34)). Equation (12) can also be extended to the multi-channel system by introducing the channel indices as,

$$\tilde{H}'\begin{pmatrix} \phi_{1,-1} \\ \phi_{2,-1} \\ \phi_{1,0} \\ \phi_{2,0} \\ \phi_{1,1} \\ \phi_{2,1} \\ \vdots \\ \phi_{1,N} \\ \phi_{2,N} \end{pmatrix} = 0,$$
(39)

with

$$\tilde{H}'_{si,s'j} = \tilde{H}_{si,s'j} - E \,\delta_{i,j}\delta_{s,s'}, \quad (i,j \ge 1), \quad (40)$$

$$\tilde{H}'_{s0,s'-1} = \tilde{H}'_{s0,s'1} = \tilde{H}'_{s1,s'0} = -t \,\delta_{s,s'},\tag{41}$$

$$\tilde{H}'_{s0,s'0} = (2t - E + \epsilon \, \delta_{s,2}) \, \delta_{s,s'},$$
 (42)

$$\tilde{H}'_{s1,s'-1} = 0. (43)$$

Notice that the dimension of  $\tilde{H}'$  is  $2(N+1) \times 2(N+2)$ . The basis functions for the Kohn variational principle can also be extended in a similar way. By arranging the wave functions as  $\psi = (\phi_{1,-1}, \phi_{2,-1}, \phi_{1,0}, \phi_{2,0}, \cdots, \phi_{1,N}, \phi_{2,N})^T$ , the basis functions are given by

$$\psi_k = (e^{-ik\Delta x}, 0, 1, 0, \dots, 0)^T,$$
 (44)

$$\psi_{-k}^{(1)} \equiv \psi_0^{(1)} = (e^{ik_1 \Delta x}, 0, 1, 0, \cdots, 0)^T,$$
 (45)

$$\psi_{-k}^{(2)} \equiv \psi_0^{(2)} = (0, e^{ik_2\Delta x}, 0, 1, 0, \dots, 0)^T, \quad (46)$$

$$\psi_n^{(1)}(i) = \delta_{i,4+2n-1},\tag{47}$$

$$\psi_n^{(2)}(i) = \delta_{i,4+2n}. \tag{48}$$

With these basis functions, the total wave function is given by

$$\Psi = \psi_k + \sum_{s=1,2} \sum_{n=0}^{N} b_{sn} \psi_n^{(s)}, \tag{49}$$

with which it is guaranteed that the incident right-going wave exists only for the channel 1. Defining the  $2(N+2) \times 2(N+1)$  wave function matrix  $\varphi_{i,sj} \equiv \psi_j^{(s)}(i)$ , the condition  $\tilde{H}'\Psi = 0$  is transformed to

$$\sum_{s'=1,2} \sum_{j=0}^{N} (\tilde{H}'\varphi)_{sl,s'j} b_{s'j} = -(\tilde{H}'\psi_k)_{sl} \equiv -\tilde{\psi}_{sl}, \quad (50)$$

from which the amplitudes  $\{b_{si}\}$  can be obtained as

$$b_{sj} = -\sum_{s'=1}^{N} \sum_{l=0}^{N} \left[ (\tilde{H}'\varphi)^{-1} \right]_{sj,s'l} \tilde{\psi}_{s'l}.$$
 (51)

The penetrability (5) is then computed as,

$$P = 1 - \sum_{s=1,2} \frac{k_s}{k_1} |b_{s0}|^2 = \sum_{s=1,2} \frac{k_s}{k_1} |b_{sN}|^2.$$
 (52)

# B. Eigenvector continuation

It is now straightforward to extend the eigenvector continuation for the single-channel problem to the multichannel problem. To this end, we first construct a vector  $\phi$  defined as

$$\phi = \sum_{s=1,2} \sum_{n=1}^{N} b_{sn} \psi_n^{(s)} \tag{53}$$

= 
$$(0,0,0,0,b_{11},b_{21},b_{12},b_{22},\cdots,b_{1N},b_{2N})^T$$
. (54)

We construct a similar function  $\phi_i$  for each of the parameter set  $\theta_i$  of the potential and superpose them to construct the total wave function as

$$\Psi = \psi_k + c_0^{(1)} \psi_{-k}^{(1)} + c_0^{(2)} \psi_{-k}^{(2)} + \sum_{i=1}^{N_{\text{EC}}} c_i \phi_i \equiv \psi_k + \sum_{i=-1}^{N_{\text{EC}}} c_i \phi_i,$$
(55)

with  $c_{-1} \equiv c_0^{(1)}$ ,  $c_0 \equiv c_0^{(2)}$ ,  $\phi_{-1} \equiv \psi_{-k}^{(1)}$ , and  $\phi_0 \equiv \psi_{-k}^{(2)}$ . From the condition of  $\tilde{H}'\Psi = 0$ , one obtains

$$\sum_{j=-1}^{N_{\rm EC}} c_j \langle \phi_i' | \tilde{H}' | \phi_j \rangle = -\langle \phi_i' | \tilde{H}' | \psi_k \rangle \equiv -d_i, \quad (56)$$

where  $\phi'_i$  and  $d_i$  are defined as  $\phi'_i \equiv \tilde{H}'|\phi_i\rangle$  and  $d_i \equiv \langle \phi'_i|\tilde{H}'|\psi_k\rangle$ , respectively, as in the single-channel problem. The coefficients  $c_i$  can then be obtained as

$$c_i = -\sum_{j=-1}^{N_{\text{EC}}} (A^{-1})_{ij} d_j, \tag{57}$$

where  $A_{ij} \equiv \langle \phi_i' | \tilde{H}' | \phi_j \rangle$ . The penetrability is then computed as

$$P = 1 - |c_{-1}|^2 - \frac{k_2}{k_1} |c_0|^2 = \left| \sum_{i=1}^{N_{\rm EC}} c_i b_{1N}^{(i)} \right|^2 + \frac{k_2}{k_1} \left| \sum_{i=1}^{N_{\rm EC}} c_i b_{2N}^{(i)} \right|^2.$$
(58)

Figure 4 shows the penetrability and the relative error as a function of energy E, for the Gaussian potentials, Eq. (1) and Eq. (32) with  $V_0 = 100$  MeV,  $F_0 = 3$  MeV, and  $s = s_f = 3$  fm. The excitation energy  $\epsilon$  is set to be 1 MeV. For the eigenvector continuation, we take  $N_{\rm EC} = 5$  and use  $F_0 = 1.5, 2.0, 2.5, 3.5,$  and 4.5 MeV while keeping

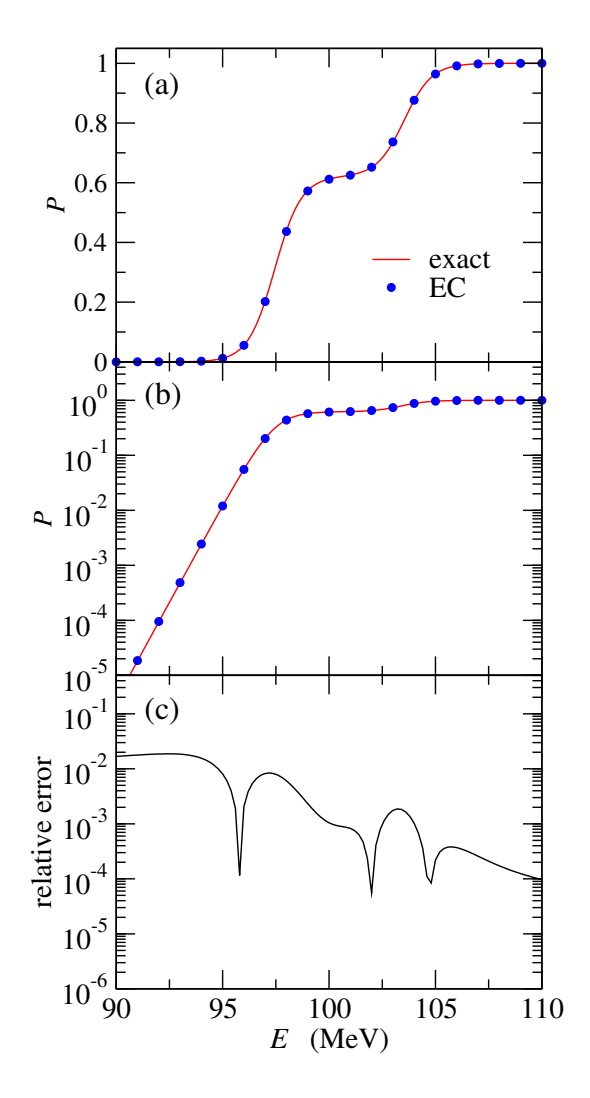


FIG. 4. Same as Fig. 2, but for the two-channel problem with the Gaussian potentials Eq. (1) and Eq. (32). The parameters of the potentials are  $V_0 = 100$  MeV,  $F_0 = 3$  MeV, and  $s_f = 3$  fm, and the excitation energy of the channel 2 is set to be  $\epsilon = 1$  MeV. For the eigenvector continuation, the number of basis vectors are taken to be  $N_{\rm EC} = 5$ , for which the strength of the coupling potential is varied as  $F_0 = 1.5$ , 2.0, 2.5, 3.5, and 4.5 MeV while keeping the values of  $V_0$ , s, and  $s_f$ .

the values of  $V_0$ , s, and  $s_f$ . That is, we vary the coupling strengths  $F_0$  between the channels 1 and 2 while keeping the diagonal potential. As in the single-channel case, one can see that the eigenvector continuation well reproduces the exact result, from well below the barrier to above the barrier. In particular, the exponential energy dependence of the penetrability at energies well below the barrier is successfully reproduced. The wave functions at  $E = V_0$  are shown in Fig. 5. The left and the right panels show the wave functions for the channel 1,  $\phi_1(x)$ , and the channel 2,  $\phi_2(x)$ , respectively. As in the single-channel problem shown in Fig. 3, one can see that the eigenvector

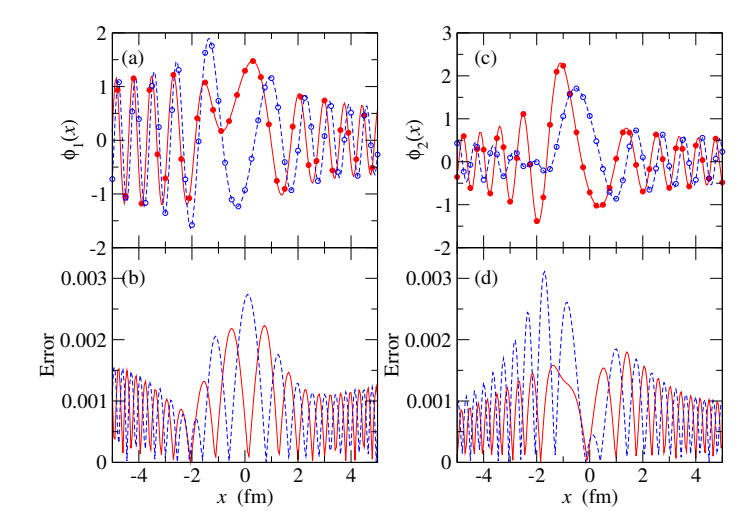


FIG. 5. Same as Fig. 3, but for the two-channel problem. See the caption of Fig. 4 for the parameters. The left and the right panels show the wave functions for the channel 1 and the channel 2, respectively.

continuation well reproduces the wave functions, for both the channels.

# IV. SUMMARY

We have constructed an emulator for a scattering problem based on the eigenvector continuation and the Kohn variational principle in the discrete basis formalism. We have applied the emulator to a multi-channel scattering problem in one-dimension with a Gaussian barrier. To implement the eigenvector continuation, for a single-channel problem we have varied the barrier height. On the other hand, for a two-channel problem, we have varied the strength of the coupling potential while keeping the barrier height. We have demonstrated that the eigenvector continuation well reproduces the exact solutions both for the single-channel and the two-channel problems. In particular, it successfully reproduces the exponential energy dependence of the penetrability at energies well below the barrier.

In this paper, we have considered a simple one-dimensional coupled-channels model. It would be straightforward to extend the emulator presented in this paper to more realistic scattering problems in three-dimension [42–44]. This will be useful e.g., in fitting experimental data to seek for optimal deformation parameters of colliding nuclei [45, 46], which requires many calculations with different values of deformation parameters. This corresponds to varying coupling strengths while keeping the diagonal potential, as we have considered in Sec. IIIB in this paper. We will report on this extension in a separate publication.

# ACKNOWLEDGMENTS

We thank G.F. Bertsch for useful discussions. This work was supported in part by the RIKEN TRIP ini-

- tiative (Nuclear Transmutation), and by JSPS KAK-ENHI Grant Numbers JP22K14030, JP23K03414, and 23KJ1212. S.Y. acknowledges JGC-Saneyoshi Scholarship Foundation.
- J. Dobaczewski, W. Nazarewicz, and P.-G. Reinhard, Error estimates of theoretical models: a guide, J. of Phys. G 41, 074001 (2014).
- [2] A. Boehnlein, M. Diefenthaler, N. Sato, M. Schram, V. Ziegler, C. Fanelli, M. Hjorth-Jensen, T. Horn, M. P. Kuchera, D. Lee, W. Nazarewicz, P. Ostroumov, K. Orginos, A. Poon, X.-N. Wang, A. Scheinker, M. S. Smith, and L.-G. Pang, Colloquium: Machine learning in nuclear physics, Rev. Mod. Phys. 94, 031003 (2022).
- [3] D. Frame, R. He, I. Ipsen, D. Lee, D. Lee, and E. Rrapaj, Eigenvector continuation with subspace learning, Phys. Rev. Lett. 121, 032501 (2018).
- [4] A. Sarkar and D. Lee, Convergence of eigenvector continuation, Phys. Rev. Lett. **126**, 032501 (2021).
- [5] T. Duguet, A. Ekström, R. J. Furnstahl, S. König, and D. Lee, Colloquium: Eigenvector continuation and projection-based emulators, Rev. Mod. Phys. 96, 031002 (2024).
- [6] A. Ekström and G. Hagen, Global sensitivity analysis of bulk properties of an atomic nucleus, Phys. Rev. Lett. 123, 252501 (2019).
- [7] S. König, A. Ekström, K. Hebeler, D. Lee, and A. Schwenk, Eigenvector continuation as an efficient and accurate emulator for uncertainty quantification, Phys. Lett. B 810, 135814 (2020).
- [8] S. Wesolowski, I. Svensson, A. Ekström, C. Forssén, R. J. Furnstahl, J. A. Melendez, and D. R. Phillips, Rigorous constraints on three-nucleon forces in chiral effective field theory from fast and accurate calculations of few-body observables, Phys. Rev. C 104, 064001 (2021).
- [9] Q. Y. Luo, X. Zhang, L. H. Chen, and J. M. Yao, Emulating the generator coordinate method with extended eigenvector continuation for the lipkin-meshkovglick model, Phys. Rev. C 110, 014309 (2024).
- [10] M. Companys Franzke, A. Tichai, K. Hebeler, and A. Schwenk, Eigenvector continuation for the pairing hamiltonian, Phys. Rev. C 109, 024311 (2024).
- [11] E. Bonilla, P. Giuliani, K. Godbey, and D. Lee, Training and projecting: A reduced basis method emulator for many-body physics, Phys. Rev. C 106, 054322 (2022).
- [12] S. Yoshida and N. Shimizu, Constructing approximate shell-model wavefunctions by eigenvector continuation, Progress of Theoretical and Experimental Physics 2022, 053D02 (2022).
- [13] T. Djärv, A. Ekström, C. Forssén, and H. T. Johansson, Bayesian predictions for a=6 nuclei using eigenvector continuation emulators, Phys. Rev. C **105**, 014005 (2022).
- [14] P. Demol, T. Duguet, A. Ekström, M. Frosini, K. Hebeler, S. König, D. Lee, A. Schwenk, V. Somà, and A. Tichai, Improved many-body expansions from eigenvector continuation, Phys. Rev. C 101, 041302 (2020).
- [15] N. Yapa, K. Fossez, and S. König, Eigenvector continuation for emulating and extrapolating two-body resonances, Phys. Rev. C 107, 064316 (2023).

- [16] R. Furnstahl, A. Garcia, P. Millican, and X. Zhang, Efficient emulators for scattering using eigenvector continuation, Phys. Lett. B 809, 135719 (2020).
- [17] C. Drischler, M. Quinonez, P. Giuliani, A. Lovell, and F. Nunes, Toward emulating nuclear reactions using eigenvector continuation, Phys. Lett. B 823, 136777 (2021).
- [18] J. Melendez, C. Drischler, A. Garcia, R. Furnstahl, and X. Zhang, Fast and accurate emulation of two-body scattering observables without wave functions, Phys. Lett. B 821, 136608 (2021).
- [19] D. Bai and Z. Ren, Generalizing the calculable r-matrix theory and eigenvector continuation to the incomingwave boundary condition, Phys. Rev. C 103, 014612 (2021).
- [20] D. Bai, New extensions of eigenvector continuation rmatrix theory based on analyticity in momentum and angular momentum, Phys. Rev. C 106, 024611 (2022).
- [21] X. Zhang and R. J. Furnstahl, Fast emulation of quantum three-body scattering, Phys. Rev. C 105, 064004 (2022).
- [22] J. Liu, J. Lei, and Z. Ren, A complex scaling method for efficient and accurate scattering emulation in nuclear reactions, Phys. Lett. B 858, 139070 (2024).
- [23] D. Odell, P. Giuliani, K. Beyer, M. Catacora-Rios, M. Y.-H. Chan, E. Bonilla, R. J. Furnstahl, K. Godbey, and F. M. Nunes, Rose: A reduced-order scattering emulator for optical models, Phys. Rev. C 109, 044612 (2024).
- [24] A. J. Garcia, C. Drischler, R. J. Furnstahl, J. A. Melendez, and X. Zhang, Wave-function-based emulation for nucleon-nucleon scattering in momentum space, Phys. Rev. C 107, 054001 (2023).
- [25] W. Kohn, Variational methods in nuclear collision problems, Phys. Rev. 74, 1763 (1948).
- [26] M. Kamimura, Chapter v. a coupled channel variational method for microscopic study of reactions between complex nuclei, Prog. Theo. Phys. Suppl. 62, 236 (1977).
- [27] Y. Mito and M. Kamimura, The generator coordinate method for composite-particle scattering based on the kohn-hulthén variational principle: Application to  $\alpha$ - $\alpha$ ,  $^{16}$ O- $\alpha$  and  $^{16}$ O- $^{16}$ O scattering, Prog. Theo. Phys. **56**, 583 (1976).
- [28] T. Matsuse, Y. Abe, and Y. Kondō, A band crossing model of resonances in heavy ion reactions. i: Resonances in <sup>12</sup>C-<sup>16</sup>O scattering, Prog. Theo. Phys. 59, 1904 (1978).
- [29] R. Beck, J. Borysowicz, D. Brink, and M. Mihailović, Variational principles for scattering in the generator coordinate method, Nucl. Phys. A 244, 45 (1975).
- [30] R. Beck, J. Borysowicz, D. Brink, and M. Mihailovlc, On calculating scattering phase shifts by the generator coordinate method, Nucl. Phys. A 244, 58 (1975).
- [31] M. A. Sharaf, A. M. Shirokov, W. Du, and J. P. Vary, Applications of the modified hulthén-kohn method for bound and scattering states (2024), arXiv:2408.05656 [nucl-th].
- [32] P. Fanto, G. F. Bertsch, and Y. Alhassid, Neutron width

- statistics in a realistic resonance-reaction model, Phys. Rev. C 98, 014604 (2018).
- [33] G. Bertsch and W. Younes, Composite-particle decay widths by the generator coordinate method, Ann. of Phys. 403, 68 (2019).
- [34] Y. Alhassid, G. Bertsch, and P. Fanto, Derivation of k-matrix reaction theory in a discrete basis formalism, Ann. of Phys. 419, 168233 (2020).
- [35] Y. Alhassid, G. Bertsch, and P. Fanto, Addendum to "derivation of k-matrix reaction theory in a discrete basis formalism" [Ann. Phys. 419 (2020) 168233], Ann. of Phys. 424, 168381 (2021).
- [36] K. Hagino, Barrier penetration with a finite mesh method, Phys. Rev. C 109, 034611 (2024).
- [37] G. F. Bertsch and K. Hagino, Barrier penetration in a discrete-basis formalism, Phys. Rev. C 109, 054606 (2024).
- [38] K. Hagino and G. F. Bertsch, Role of momentum in the generator-coordinate method applied to barrier penetration, Phys. Rev. C 110, 054610 (2024).
- [39] C. Dasso, S. Landowne, and A. Winther, Channel-coupling effects in heavy-ion fusion reactions, Nucl. Phys. A 405, 381 (1983).
- [40] C. Dasso, S. Landowne, and A. Winther, A study of q-value effects on barrier penetration, Nucl. Phys. A 407, 221 (1983).
- [41] K. Hagino and A. B. Balantekin, WKB approximation for multichannel barrier penetrability, Phys. Rev. A 70,

- 032106 (2004).
- [42] K. Hagino, N. Rowley, and A. Kruppa, A program for coupled-channel calculations with all order couplings for heavy-ion fusion reactions, Comput. Phys. Comm. 123, 143 (1999).
- [43] K. Hagino and N. Takigawa, Subbarrier fusion reactions and many-particle quantum tunneling, Prog. Theo. Phys. 128, 1061 (2012).
- [44] K. Hagino, K. Ogata, and A. Moro, Coupled-channels calculations for nuclear reactions: From exotic nuclei to superheavy elements, Prog. in Part. and Nucl. Phys. 125, 103951 (2022).
- [45] Y. Gupta, B. Nayak, U. Garg, K. Hagino, K. Howard, N. Sensharma, M. Şenyiğit, W. Tan, P. O'Malley, M. Smith, R. Gandhi, T. Anderson, R. deBoer, B. Frentz, A. Gyurjinyan, O. Hall, M. Hall, J. Hu, E. Lamere, Q. Liu, A. Long, W. Lu, S. Lyons, K. Ostdiek, C. Seymour, M. Skulski, and B. Vande Kolk, Determination of hexadecapole (β<sub>4</sub>) deformation of the light-mass nucleus <sup>24</sup>Mg using quasi-elastic scattering measurements, Phys. Lett. B 806, 135473 (2020).
- [46] Y. Gupta, V. Katariya, G. Prajapati, K. Hagino, D. Patel, V. Ranga, U. Garg, L. Danu, A. Pal, B. Joshi, S. Dubey, V. Desai, S. Panwar, N. Kumar, S. Mukhopadhyay, P. Singh, N. Sirswal, R. Sariyal, I. Mazumdar, and B. John, Precise determination of quadrupole and hexadecapole deformation parameters of the sd-shell nucleus, <sup>28</sup>Si, Phys. Lett. B 845, 138120 (2023).